Chemical Engineering Journal 160 (2010) 432–439

Contents lists available at ScienceDirect

Chemical Engineering Journal

journal homepage: www.elsevier.com/locate/cej

Manganese dioxide nanowhiskers: A potential adsorbent for the removal of Hg(II) from water

K.P. Lisha, Shihabudheen M. Maliyekkal, T. Pradeep*

Department of Chemistry and Sophisticated Analytical Instrument Facility, Indian Institute of Technology Madras, Chennai 600036, India

ARTICLE INFO

Article history:
Received 5 December 2009
Received in revised form 11 March 2010
Accepted 16 March 2010

Keywords:
Adsorption
Chlor-alkali industrial effluent
Hg(II)
Manganese dioxide nanowhiskers
Water

ABSTRACT

Manganese dioxide nanowhiskers (MDN), prepared by the reduction of potassium permanganate by ethyl alcohol has been investigated as an adsorbent for Hg(II) removal from aqueous medium. Characterization of the as-synthesized material was carried out using transmission electron microscopy (TEM), scanning electron microscopy (SEM), energy dispersive analysis of X-rays (EDAX), X-ray photoelectron spectroscopy (XPS), and X-ray diffraction (XRD). SEM and TEM data showed that the as-synthesized MDN looks like agglomerated whiskers of 5–10 nm in diameter and 100–300 nm in length. XRD data revealed the formation of birnessite type layered manganese dioxide. Mn(IV) oxidation state of Mn in MDN was confirmed by XPS. Batch experiments were conducted to evaluate the Hg(II) adsorption capacity of MDN. Hg(II) adsorption on MDN is a fast process and the kinetics followed a pseudo-second-order rate equation. The Hg(II) uptake varied with pH and showed optimum performance at pH 6–9. The experimental evidence revealed that physisorption is the dominating mechanism in Hg(II) removal. Considering the practical difficulty in handling nanomaterials, MDN was supported on Al_2O_3 (MDN@Al_2O_3) and the composite was shown to be an efficient adsorbent for Hg(II) from simulated chlor-alkali industrial effluent. The results suggest that this material can be a practical solution for Hg(II) scavenging in several industrial processes.

1. Introduction

Mercury is a toxic heavy metal widely used in industries related to chlor-alkali, pharmaceuticals, manufacturing of pressure and temperature measurement devices, mining and dental implants. Effluent discharges from these industries exhibit wide distribution in concentration and composition of mercury [1,2]. Once released into the environment, mercury can undergo complex physical, chemical, and biological transformations and can accumulate in the food chain and cause neurological, nephrological, reproductive, and genetic disorders in humans [3]. A recent study on the status of mercury in ground water in various states of India showed an alarming situation. Drinking water sample from Panipat industrial area (Haryana, India) showed the highest level, 268 times the upper safe limit [4]. These higher levels are due to the discharge of mercury bearing effluents having concentrations above the permissible limit of 0.01 mg L^{-1}.

Technologies like ion exchange [5], amalgamation [6] and adsorption [7] are reported for Hg(II) removal from wastewater. Adsorption technology has been widely accepted because of its effectiveness, efficiency and economics. Metal oxides possess higher adsorption capacity, metal ion affinity, and ability to remove metals in trace concentrations with the possibility of recovery and reuse [8]. Oxides of manganese are considered to be one of the most important scavengers of aqueous trace metals and have been extensively studied for the removal of various toxic heavy metal pollutants such as As [9], Pb [10], Cd [11], Cu [12], and Ni [13] from drinking as well as wastewater. Apart from their excellent heavy metal uptake capacity, they are also interesting because of low cost, eco-friendly nature and abundant availability. Surprisingly, very limited studies have been carried out to explore the ability of manganese oxide to remove Hg(II) from aqueous medium. The reported studies on Hg(II) removal by manganese oxides showed a wide variation in adsorption capacity (0.13–113 mg g^{-1}) [14–16]. Though these data are obtained at various experimental conditions and they are not necessarily comparable, the data clearly show the importance of synthetic route and the crystal structure of the manganese oxide in Hg(II) uptake. Besides, to the best of our knowledge, no mechanistic and surface binding details of Hg(II) on MnO_2 are available in the literature.

Recent findings show that nanomaterials are highly promising in water purification process due to their unique properties like higher surface area per unit volume, ease with which they can be anchored onto solid matrices and the ability to functionalize with different functional groups to enhance their affinity towards target molecules [17]. A recent study by Subramanian et al. [18]

* Corresponding author. Tel.: +91 44 2257 4208; fax: +91 44 2257 0545.
E-mail address: pradeep@iitm.ac.in (T. Pradeep).

1385-8947/$ – see front matter © 2010 Elsevier B.V. All rights reserved.
doi:10.1016/j.cej.2010.03.031

has proposed a simple, low cost, fast, and eco-friendly method for the preparation of nanostructured manganese oxide. This approach requires only one starting manganese precursor, $KMnO_4$, simplifying the post-synthesis treatment and thereby increasing the viability in commercial applications. In one such approach, where manganese oxide nanospheres were synthesized by the reaction between potassium permanganate and oleic acid and was tested for its Hg(II) removal capacity [19]. The uptake was found to be less (0.84 mg g^{-1}) and may be due to the hausmannite structure, which clearly indicates the importance of reducing agent and post-synthesis treatment of the product.

In the present study, manganese dioxide nanowhiskers (MDN), prepared by the reaction of potassium permanganate and ethyl alcohol, was tested for its Hg(II) uptake in detail. Various spectroscopic and microscopic examinations were done to characterize the material and evaluate its performance for Hg(II) uptake. The surface binding details of Hg(II) on MDN was established through spectroscopy, coupled with adsorption experiments. Considering the practical difficulties in handling free standing nanomaterials, studies were extended to immobilize the MDN on micron size alumina particles (MDN@Al_2O_3). The utility of the as-prepared composite material were demonstrated by cleaning-up Hg(II) from a synthetically prepared industrial effluent of practical significance (chlor-alkali industrial effluent). Regeneration and reusability of the supported adsorbent was also studied to evaluate the economics of the adsorbent as the Hg(II) removal medium.

2. Materials and methods

2.1. Materials

Chemicals used in this study were of analytical grade. Potassium permanganate and ethyl alcohol were procured from Merck Ltd., India and Jiangsu Huaxi International Trade Co.-Ltd., China, respectively. Rhodamine 6G was purchased from Fluka Chemicals, Switzerland. A stock solution of 1000 mg L^{-1} Hg(II) was prepared from mercuric chloride (Glaxo Laboratories Ltd., India) using distilled water. Required concentrations of the samples were prepared by serial dilutions of the stock solution. Neutral activated aluminium oxide was purchased from Maharashtra Chemical Products, India and particles below 100 μm in size were collected by screening.

2.2. Preparation of MDN and MDN@Al_2O_3

MDN was synthesized by the reaction between potassium permanganate and ethyl alcohol, similar to a procedure reported by Subramanian et al. [18]. In this method, 0.5 g of potassium permanganate was dissolved in 300 mL of distilled water. 10 mL of ethyl alcohol was added drop-wise to the above solution while stirring. A brownish-black precipitate, which formed was filtered and washed thoroughly to remove any byproducts. The product obtained was dried at 60 °C overnight, ground well and stored in an airtight container for further use. For the synthesis of MDN@Al_2O_3, 20 g of Al_2O_3 was soaked in 30 mL of 0.01 M potassium permanganate for 2 h and 10 mL of ethyl alcohol was added drop-wise while stirring. The product was separated from the solution by appropriate screening, washed thoroughly and dried at 60 °C overnight.

2.3. Characterization of the adsorbents

TEM was carried out using a JEM 3010, 300 kV instrument with an ultra high resolution (UHR) polepiece (JEOL, Japan). The samples for TEM were prepared by dropping the sample dispersion on amorphous carbon films supported on a copper grid and dried in ambience. Surface morphology and elemental analysis of the as-prepared samples were done using a SEM equipped with EDAX (FEI QUANTA-200 SEM, Czechoslovakia). For this, the samples were drop-casted on an indium tin oxide (ITO) conducting glass and dried. XRD data were collected with an X-ray diffractometer (Bruker AXS, D8 Discover, USA) using Cu-Kα radiation (λ = 1.54 Å). The samples were scanned in the 2θ range of 10–90°. The XPS measurements were conducted using an Omicron ESCAProbe spectrometer (Omicron Nanotechnology, Taunusstein, Germany), with monochromatized Mg Kα X-rays ($h\nu$ = 1253.6 eV). The specimens were prepared as drop cast films on a sample stub and a constant analyzer energy of 20 eV was used for the measurements. The amount of manganese coated on MDN@Al_2O_3 was quantified by acid digestion method suggested by national environment protection council [20]. The concentration of manganese was measured using atomic absorption spectrophotometer (PerkinElmer, AA analyst 700, USA) and a hollow cathode lamp (HCL).

Table 1
Composition of simulated chlor-alkali industrial effluent.

Parameters (mg L^{-1})	Quantity
pH@25 °C	8.6
Hg(II)	20.0
Pb(II)	2.2
Cd(II)	1.1
Mg(II)	33.2
Ca(II)	51.1
Na(I)	241.6
Cl^-	379.2
NO_3^-	343.5
PO_4^{3-}	19.0
NH_4^+	31.5
BOD_5	79.0
Conductivity (mS cm^{-1})	19.6

2.4. Hg(II) uptake studies

Hg(II) batch adsorption experiments were carried out in 250 mL glass conical flasks. The working volume of the solution was taken as 100 mL at pH 5.5 (±0.2) and dose of MDN was maintained as 10 mg. The flasks were kept for shaking at 160 ± 5 rpm in an orbital shaker (Riviera, India) at 30 ± 2 °C. Samples were withdrawn at predetermined time intervals and residual concentration of Hg(II) was detected using a PerkinElmer Lambda 25 UV–vis absorption spectrometer, USA [7]. For detection, the sample, KI buffer and Rhodamine 6G solutions were added in 2:1:1 ratio. For detecting residual concentrations of Hg(II) below 0.2 mg L^{-1}, all samples were concentrated 20 times. Effect of contact time on Hg(II) uptake was studied for 10, 20, 30 and 40 mg L^{-1} Hg(II). The samples were collected at specific time intervals for residual Hg(II) analysis. Equilibrium studies were performed as a function of temperature (20, 30 and 40 °C). The Hg(II) concentrations were varied over a range of 10–40 mg L^{-1}. The samples were collected after the equilibrium contact time of 1 h and analyzed for residual Hg(II) concentrations. Effect of adsorbent dose (2.5–100 mg) was investigated for 10 mg L^{-1} Hg(II). Hg(II) uptake was also investigated as a function of pH by varying it from around 2–10 and at an initial Hg(II) concentration of 20 mg L^{-1}. The initial pHs of the samples were adjusted using dilute NaOH or HCl solution.

2.5. Application for the treatment of simulated chlor-alkali industrial effluent

Chlor-alkali industrial effluent was simulated (Table 1) and the effect of adsorbent dose on Hg(II) removal was studied using MDN and MDN@Al_2O_3. A control experiment was carried out using Al_2O_3. The economic viability of any adsorbent depends upon

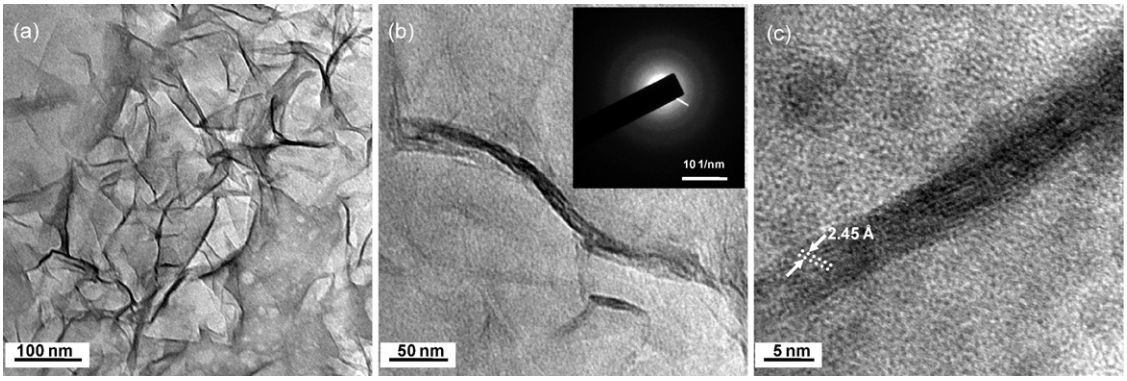

Fig. 1. TEM images of MDN at various magnifications. (a) Large area image, (b) single whisker, and (c) lattice resolved image. Inset of (b) shows the SAED pattern taken from a whisker.

its reuse capacity for repeated cycles of adsorption. In order to test the reusability of MDN@Al_2O_3, three consecutive cycles of adsorption–desorption studies were carried out. To start with, adsorption studies were initially carried out with MDN@Al_2O_3 (0.5 g) as described earlier. Hg(II) loaded adsorbent was collected and washed with distilled water to remove any unbound Hg(II). The Hg(II) loaded samples were treated with various concentration of HCl (0.05–0.5 M) for 1 h to find the optimum eluent concentration. To test the reusability of MDN@Al_2O_3, the adsorption–desorption cycle was repeated for three consecutive cycles with an optimum eluent concentration (0.2 M HCl).

3. Results and discussion

3.1. Characterization of the adsorbents

TEM micrographs of MDN before and after reaction with Hg(II) were investigated for understanding the morphology. Fig. 1a shows a large area TEM micrograph of freshly prepared MDN. The particles formed are whisker shaped nanoscale-structures with certain degree of aggregation. Fig. 1b shows the magnified view of a single whisker. The whiskers formed are 100–300 nm in length and 5–10 nm in diameter. The weak crystalline nature of MDN is observable from the high resolution TEM image shown in Fig. 1c and the SAED (selected area electron diffraction) pattern shown in the inset of Fig. 1b. A lattice spacing of 2.45 Å is seen, which corresponds to the (1 0 0) plane of layered birnessite. Fig. S1 of Supplementary data shows the large area TEM micrograph of Hg(II) treated MDN, the degree of aggregation is more after Hg(II) adsorption.

Figs. S2a and S2b of Supplementary data are large area SEM images of freshly prepared MDN and Hg(II) treated MDN, respectively. Aggregated morphology of the material is observable in Fig. S2a. After Hg(II) adsorption, the extent of aggregation increases. Fig. S2d–f are the elemental maps of Mn, O and Hg of the Hg(II) loaded MDN sample. The corresponding EDAX spectrum and elemental composition are shown in Fig. S2g. From the elemental analysis, it is clear that a significant amount of Hg is present in the sample and is uniformly distributed. Fig. S3 of Supplementary data shows the SEM micrographs of pristine Al_2O_3 and MDN@Al_2O_3 particle surfaces. The surface of Al_2O_3 is highly irregular with many projections and cracks (Fig. S3a). The surface morphology of Al_2O_3 changes after loading MDN and is shown in Fig. S3c. From the SEM data, it is also visible that MDN is distributed more or less uniformly on Al_2O_3 surface. The presence and uniform loading of MDN on Al_2O_3 is confirmed by the elemental mapping (Fig. S4 of Supplementary data). The presence of Mn on Al_2O_3 is also confirmed from the EDAX spectrum and composition table shown in Fig. S4.

XRD analyses were performed to examine the crystal structure and phase purity of MDN and Hg(II) loaded MDN. In Fig. S5 of Supplementary data, panel 'a' shows the XRD pattern of freshly prepared MDN. The powder found to be poorly crystallized with broad peaks at 23.27°, 37.19° and 66.63° in 2θ. These peaks correspond to (0 0 2), (1 0 0) and (1 1 0) planes of layered birnessite [21]. The XRD data is in accordance with TEM data. Panel 'b' in Fig. S5 shows the XRD pattern of Hg(II) loaded MDN. All the three (0 0 2), (1 0 0) and (1 1 0) planes of birnessite are present indicating the absence of structural modification of the pristine sample. The peak observed around 30.46° in 2θ may be attributed to (0 1 1) plane of adsorbed HgO [JCPDS: 73-1564] on MDN surface. The peaks become narrow after Hg(II) adsorption and it may be due to the increase in crystallinity.

XPS analyses were performed to understand the chemical state of MDN before and after reaction with Hg(II). Fig. 2A shows the XPS survey scan of freshly prepared MDN and MDN exposed to Hg(II) for 1 h. The photoelectron peaks reveal that the nanoparticle surface consists mainly of manganese and oxygen, and small amounts of carbon. Carbon on MDN surface may be due to some impurities. In the Hg(II) loaded sample, in addition to Mn, O and C, the peak of Hg are evident. Detailed XPS scan for Mn 2p and O 1 s regions before and after Hg(II) exposure are shown in Fig. 2B and C, respectively. XPS spectrum for Mn 2p before Hg(II) exposure shows peaks at 642.1 and 653.9 eV, close to $2p_{3/2}$ and $2p_{1/2}$ of Mn(IV) [22]. The Mn 2p peak obtained for the Hg(II) loaded sample is similar to the pristine sample and the binding energy data are close to Mn in Mn(IV) sate. It is a clear evidence for the absence of chemical modification of MDN after Hg(II) adsorption. Fig. 2C shows the detailed XPS scans for O 1 s before and after Hg(II) adsorption and both show photoelectron peak at 529.7 eV, corresponding to the O^{2-} binding energy. Fig. 2D is the XPS spectrum in the Hg 4f region and the peaks at 100.6 and 104.6 eV correspond to the binding energies ($4f_{7/2}$ and $4f_{5/2}$) of oxidized mercury [Hg(II)] in HgO [23].

The manganese present in MDN@Al_2O_3 system was quantified by acid digestion method. It was found that 5.47 mg of Mn is present per gram of MDN@Al_2O_3.

3.2. Hg(II) uptake studies

3.2.1. Effect of solution pH on adsorption

Solution pH is an important parameter that influences most of the adsorption system. Studies were performed on Hg(II) removal by MDN at various solution pH ranging from 2–10 and the results obtained are depicted in Fig. 3. Hg(II) adsorption was found to be pH dependent and the uptake is less at low pH. However, with the increase in pH from 2.0 to 10, a significant enhancement in adsorption is observed. The optimum pH for Hg(II) uptake was recorded

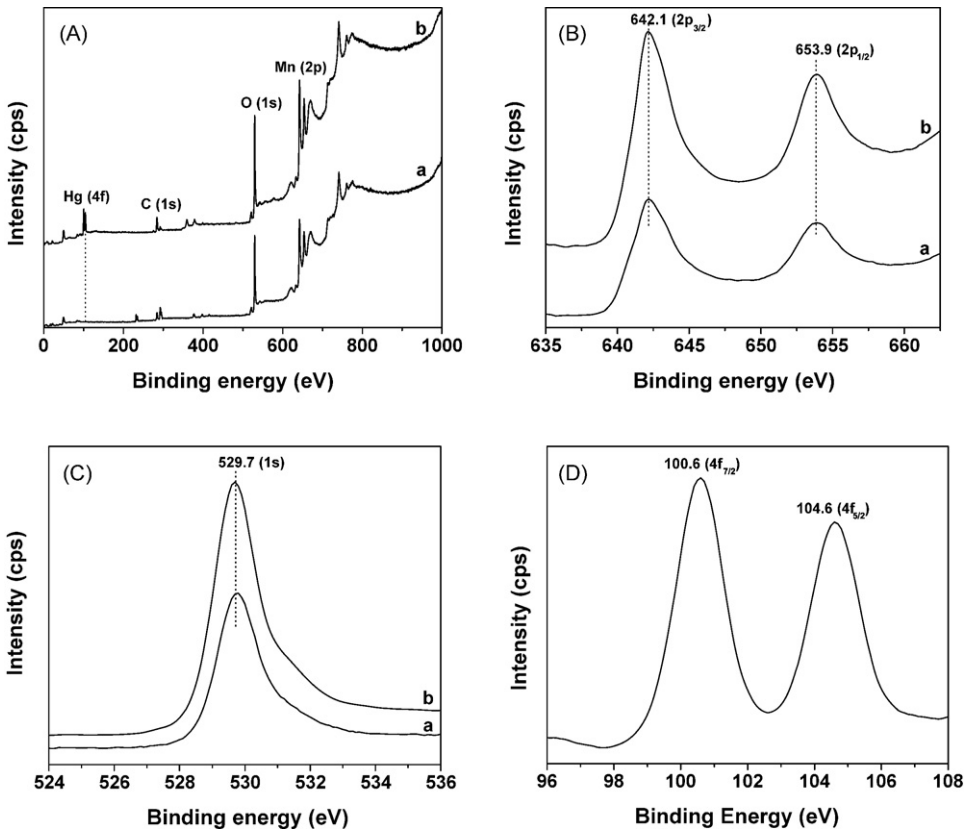

Fig. 2. XPS spectra of MDN. (A) survey scan, (B) Mn 2p region, (C) O 1s region, ((D) Hg 4f region after adsorption on MDN. The spectra (a) and (b) correspond to pristine and Hg(II) adsorbed MDN, respectively. The traces are shifted vertically for clarity.

at pH range of 6–9.

3.2.2. Effect of adsorbent dosage

The Hg(II) adsorption capacity of MDN as a function of adsorbent dose was studied and the result is shown in Fig. 4. The initial Hg(II) concentration was maintained at 10 mg L^{-1}. As expected, the amount of Hg(II) adsorbed increased with increase in MDN dose from 2.5 mg to 10.0 mg. This can be attributed to the increase in the available reaction sites with increase in the MDN dose [24]. When the MDN dose was further increased, there was less proportionate increase in adsorption. This may be due to the unsaturation of the available adsorption sites and increased particulate interaction, and thus leading to agglomeration of the particles. For a comparison, the same experiment was repeated with bulk manganese dioxide (MDB) and it showed very poor Hg(II) removal potential, 28.5% for an adsorbent dose of 100 mg. The reduced Hg(II) removal potential of MDB may be due to the less number of reactive sites per unit area of bigger particles.

Effect of initial Hg(II) concentration on the distribution coefficient K_d, L g^{-1} (Eq. (1)) is shown in Fig. S6 of supplementary data.

$$K_d = \frac{(C_0 - C_e)}{C_e} \times \frac{V}{m} \quad (1)$$

where C_0 and C_e (mg L^{-1}) are the initial and equilibrium concentrations of Hg(II) in solution, V (L) is the solution volume and m (g) is the mass of the adsorbent. K_d values decreased with increasing concentration of Hg(II). At low metal ion/adsorbent ratios, metal ion adsorption involves higher energy sites. As the metal ion/adsorbent ratio increases, the higher energy sites are saturated and adsorp-

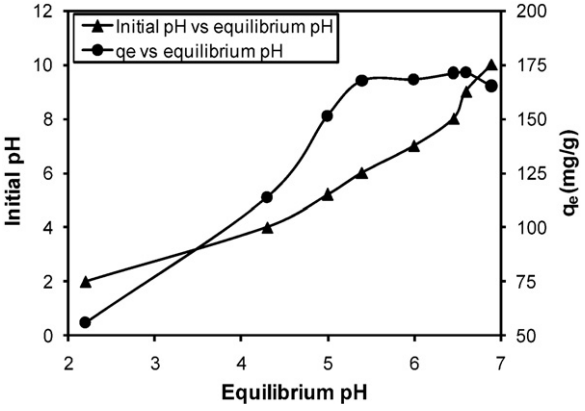

Fig. 3. Effect of pH on the adsorption of Hg(II) by MDN. Initial Hg(II) concentration = 20 mg L^{-1}.

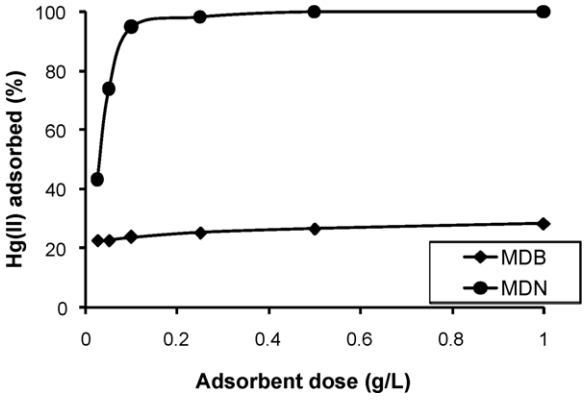

Fig. 4. Effect of adsorbent dose on Hg(II) removal by MDN and MDB. Initial Hg(II) concentration = 10 mg L^{-1}.

Table 2
Pseudo-first-order and pseudo-second-order reaction kinetic parameters obtained for the adsorption of Hg(II) by MDN.

Hg(II) (mg L^{-1})	Pseudo-first-order rate parameters			Pseudo-second-order rate parameters			
	k_1 (min^{-1})	q_e (mg g^{-1})	R^2	k_2 (g mg^{-1} min^{-1})	q_e	h	R^2
10.0	1.8×10^{-2}	13.5	0.954	8.0×10^{-3}	100.0	83.3	0.999
20.0	2.9×10^{-2}	23.9	0.931	5.0×10^{-3}	142.9	100.0	0.999
30.0	1.6×10^{-2}	27.2	0.860	4.9×10^{-3}	166.7	125.0	0.999
40.0	1.4×10^{-2}	21.0	0.872	4.0×10^{-3}	200.0	166.7	0.999

tion begins at lower energy sites and results in decreasing K_d values. The observed K_d values varies from (9–190) $\times 10^3$ mL g^{-1} for 10–40 mg L^{-1} Hg(II), and it indicates a successful separation process [25].

3.2.3. Adsorption kinetics

Effect of contact time between adsorbent and Hg(II) was studied as a function of initial Hg(II) concentration and the results are shown in Fig. S7 of Supplementary data. The adsorption of Hg(II) on MDN is very fast and most of the adsorption happens in the initial contact period of 2.5 min. Thereafter, the uptake rate reduces significantly and a pseudo-equilibrium value is reached in 30 min.

3.2.3.1. Kinetic data analysis. In order to understand the system better, the kinetic data were initially analyzed using two reaction models; pseudo-first-order [26] and pseudo-second-order [27] models. The mathematical representations (linear form) of these models are given in Eqs. (2) and (3), respectively.

Pseudo-first-order reaction equation:

$$\log(q_e - q_t) = \log(q_e) - \frac{k_1 t}{2.303} \tag{2}$$

Pseudo-second-order reaction equation:

$$\frac{t}{q_t} = \frac{1}{h} + \frac{t}{q_e} \tag{3}$$

$$h = k_2 q_e^2 \tag{4}$$

where q_e and q_t (mg g^{-1}) are the amount of metal ion adsorbed at equilibrium and at time t, respectively. k_1 (min^{-1}) and k_2 (g mg^{-1} min^{-1}) are the first-order and second-order rate constant for the adsorption, and h is the initial adsorption rate (mg g^{-1} min^{-1}). The kinetic plots generated by pseudo-first-order and pseudo-second-order equations along with the experimental kinetic plots are given in Fig. S8 of supplementary data and Fig. 5, respectively. The kinetics parameters obtained from these model fits are summarized in Table 2. The fit with pseudo-second-order equation is better as evident from the high coefficient of determination (R^2) value.

3.2.4. Adsorption equilibrium

To estimate adsorption capacity, the equilibrium data were fitted to the well-known Langmuir, Freundlich and Sips isotherm models. The mathematical representations of these models are given in Eqs. (5)–(7) and the details are given elsewhere [28].

Langmuir model:

$$q_e = \frac{q_L b_L C_e}{1 + b_L C_e} \tag{5}$$

Freundlich model:

$$q_e = K_F C_e^{1/n} \tag{6}$$

Sips model:

$$q_e = \frac{q_s K_s C_e^{m_s}}{1 + K_s C_e^{m_s}} \tag{7}$$

where q_L (mg g^{-1}) and b_L (L mg^{-1}) are the Langmuir monolayer adsorption capacity and isotherm constant, respectively. K_F (mg$^{1-1/n}$ L$^{1/n}$ g^{-1}) and n are the Freundlich isotherm constant and adsorption intensity, respectively. q_s (mg g^{-1}), K_s (L g^{-1}) and m_s are the specific adsorption capacity of Sips equation at saturation, Sips isotherm constant and Sips isotherm exponent, respectively.

Fig. 6 shows the isotherm plots obtained for the adsorption of Hg(II) by MDN at 303 K. The isotherm plots obtained at 293K and 313 K are shown in Fig. S9 of Supplementary data. The estimated isotherm parameters from these model fits are summarized in Table 3. The experimental data fitted well with the Langmuir model, which is evident from the high R^2 value. It is found that the maximum Hg(II) adsorption capacity of MDN is 199.53 mg g^{-1}, which is considerably higher than 0.13–133 mg g^{-1}, the reported Hg(II) uptake capacities of MnO_2 prepared through other synthetic methods [14–16].

The essential characteristics and the feasibility of the Langmuir isotherm can be explained in terms of a dimensionless constant separation factor or equilibrium parameter R_L, which is defined by

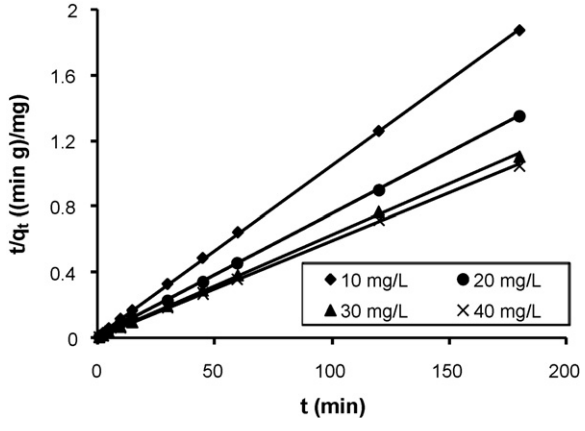

Fig. 5. Pseudo-second-order reaction kinetic plots for the adsorption of Hg(II) by MDN.

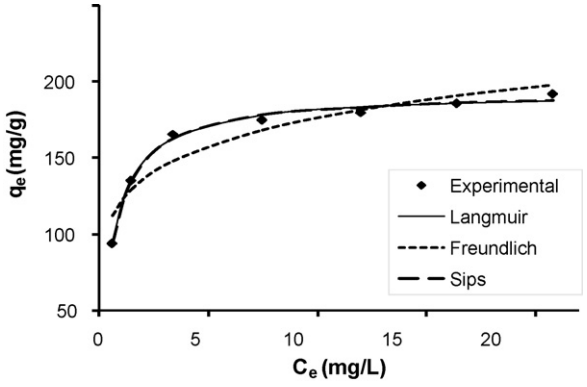

Fig. 6. Various isotherm model fits for the adsorption of Hg(II) by MDN at 303 K.

Table 3
Isotherm parameters obtained for the adsorption of Hg(II) by MDN.

T (K)	Freundlich isotherm parameters			Langmuir isotherm parameters			Sips isotherm parameters			
	K_F ($mg^{1-1/n} L^{1/n} g^{-1}$)	n	RMSE	q_L ($mg\,g^{-1}$)	b ($L\,mg^{-1}$)	RMSE	K_s ($L\,g^{-1}$)	q_s ($mg\,g^{-1}$)	m_s	RMSE
293.0	113.3	6.0	9.70	184.8	1.3	5.39	1.3	186.3	0.95	5.38
303.0	122.0	6.3	10.60	193.3	1.6	2.71	1.6	193.5	0.99	2.54
313.0	122.6	5.7	8.29	199.5	1.6	6.05	1.4	219.8	0.67	4.65

Table 4
Thermodynamic parameters obtained for the adsorption of Hg(II) by MDN.

Hg(II) ($mg\,L^{-1}$)	ΔH° ($J\,mol^{-1}$)	ΔS° ($J\,(mol\,K)^{-1}$)	K_c			$-\Delta G^\circ$ ($J\,mol^{-1}$)		
			293.0 (K)	303.0 (K)	313.0 (K)	293.0 (K)	303.0 (K)	313.0 (K)
30.0	5296.1	40.0	14.0	15.0	16.1	6429.9	6826.7	7230.5
35.0	8763.6	49.0	9.9	11.3	12.4	5582.3	6118.8	6560.5

Eq. (8) [29].

$$R_L = \frac{1}{1 + b_L C_0} \tag{8}$$

Based on the R_L values, one can assess the behavior of the equilibrium to be favorable ($0 < R_L < 1$), unfavorable ($R_L > 1$), irreversible ($R_L = 0$) or linear ($R_L = 1$). For adsorption of Hg(II) on MDN, R_L values obtained are shown in Fig. S10 of Supplementary data. The R_L values for various initial concentrations of Hg(II) are found to be in the range 0.015–0.069, indicating that adsorption is a favorable process.

3.2.4.1. Adsorption thermodynamics. To understand the variation in the extent of adsorption with respect to temperature, the thermodynamic parameters: changes in standard free energy (ΔG°, $J\,mol^{-1}$), enthalpy (ΔH°, $J\,mol^{-1}$) and entropy (ΔS°, $J\,mol^{-1}\,K^{-1}$) have been calculated using the following thermodynamic relations [30] (Eqs. (9)–(12)).

$$\Delta G^\circ = \Delta H^\circ - T\Delta S^\circ \tag{9}$$

$$\Delta G^\circ = -2.303RT \log K_c \tag{10}$$

$$K_c = \frac{q_e}{C_e} \tag{11}$$

$$\log \frac{q_e}{C_e} = \frac{\Delta S^\circ}{2.303R} - \frac{\Delta H^\circ}{2.303R}\frac{1}{T} \tag{12}$$

where T (K) is the absolute temperature, K_c is the equilibrium constant and R ($8.314\,J\,K^{-1}\,mol^{-1}$) is the universal gas constant, respectively.

The values of ΔS° and ΔH° are computed from the slope and intercept of the plot (Supplementary Fig. S11). ΔG° at various temperatures has also been calculated by using Eq. (10). The thermodynamic parameters thus calculated are listed in Table 4. Positive values of ΔH° suggest the endothermic nature of Hg(II) adsorption on MDN. Increase in entropy of the adsorption reaction is shown by positive values of ΔS° and the negative values of ΔG° indicating that the adsorption is spontaneous in nature [31].

3.2.4.2. Free energy of adsorption. Most of the isotherm equations, including Langmuir and Freundlich isotherms, do not explain the adsorption mechanism. However, Dubinin–Radushkevich (D–R) isotherm can be used to find the free energy of adsorption and hence the adsorption mechanism [28]. The mean free energy of adsorption (E_{DR}, $kJ\,mol^{-1}$), defined as free energy change when 1 mol of ion is transferred from infinity in solution to the surface of the solid, and can be estimated using the following expressions (Eqs. (13)–(15)).

$$E_{DR} = \frac{1}{(2\beta)^{1/2}} \tag{13}$$

$$\ln q_e = \ln q_m - \beta\varepsilon^2 \tag{14}$$

$$\varepsilon = RT \ln\left(1 + \frac{1}{C_e}\right) \tag{15}$$

where β ($mol^2\,kJ^{-2}$) is the constant of D–R isotherm, ε is the Polanyi potential and q_m ($mol\,kg^{-1}$) is the adsorption capacity.

A straight line plot of $\ln(q_e)$ vs ε^2 in Fig. S12 of supplementary data can be used to find β and hence the mean free energy of adsorption. The value of E_{DR} found in this study was $2.32\,kJ\,mol^{-1}$, signifying that a physical electrostatic force was potentially involved in the adsorption process [32].

3.3. Application for the treatment of simulated chlor-alkali industrial effluent

The chlor-alkali industrial effluent was simulated [33] and the Hg(II) removal from such effluent was demonstrated. In order to avoid any practical difficulties, such as poor solid-liquid separation and low hydraulic conductivity, which can arise from using nanopowders as adsorbent, MDN@Al_2O_3 granules was prepared and tested in the lab. Fig. 7 shows the effect of MDN@Al_2O_3 dose on the Hg(II) uptake from $20\,mg\,L^{-1}$ Hg(II) spiked distilled water and simulated industrial effluent. As clear from the data, the percentage removal of Hg(II) by MDN@Al_2O_3 increases with increase in adsorbent dose. However, a clear difference in Hg(II) uptake pattern was observed with Hg(II) spiked distilled water and simulated industrial effluent. As expected, the removal efficiency in the latter case was reduced significantly. The other heavy metals present in the simulated industrial effluent (Pb and Cd) were also tested. The result shows more than 99% removal of the Pb(II) and Cd(II) form the solution. In order to evaluate the Hg(II) uptake capacity

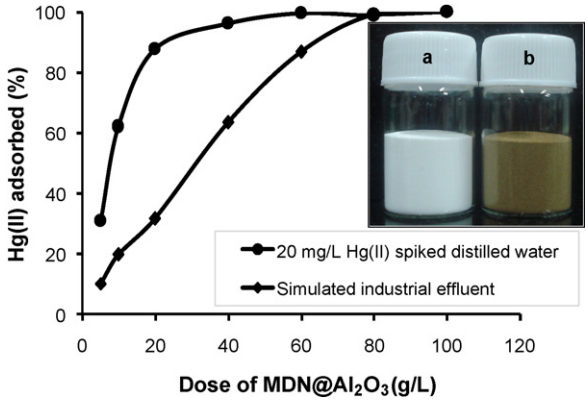

Fig. 7. Effect of MDN@Al_2O_3 dose on Hg(II) removal. Inset: photographs of (a) Al_2O_3 and (b) MDN@Al_2O_3.

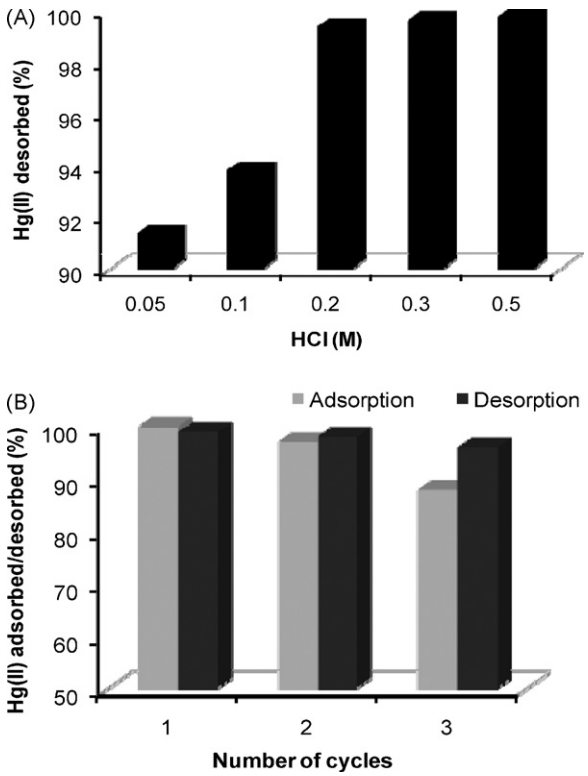

Fig. 8. Regeneration of MDN@Al_2O_3. (A) Effect of HCl concentration on Hg(II) desorption and (B) Hg(II) adsorption and desorption efficiency (%) in different cycles.

of parent Al_2O_3 and its overall contribution in adsorption process, we have also studied the Hg(II) adsorption capacity of parent Al_2O_3 and the data is shown in Supplementary Fig. S13. The results reveal that MnO_2@Al_2O_3 is superior to parent alumina in removing Hg(II) from both industrial effluent as well as Hg(II) spiked distilled water.

3.4. Regeneration of MDN@Al_2O_3

Economic viability of any adsorption process depends upon the reusability of the adsorbents for number of cycles of adsorption process. A study was conducted to evaluate the reuse potential of MDN@Al_2O_3. HCl was used as an eluent to desorb the adsorbed Hg(II) from the material. Fig. 8A shows the effect of eluent (HCl) concentration on Hg(II) desorption. It is observed that 0.2 M HCl could elute more than 99% adsorbed Hg(II). To test the adsorption potential of regenerated MDN@Al_2O_3, two more cycles of adsorption–desorption studies were carried out and the data is shown in Fig. 8B. The experimental conditions were unaltered throughout the cycles. The result reveals that MDN@Al_2O_3 has excellent reuse potential and only 4% reduction in Hg(II) uptake capacity was observed at the end of the third cycle. The data clearly shows that MDN is a promising candidate for the adsorption of Hg(II) from aqueous medium. However, more exhaustive studies are required to find an effective support and life of the adsorbent so as to achieve optimum performance.

3.5. Discussion on the adsorption mechanism

The behavior of Hg(II) in aqueous solutions is complex and can present in different compositions with varying degrees of activity. Under different pH conditions Hg(II) can present as hydrolyzed ions of varying compositions. The Hg(II) exists as the dominant species in the solution at pH < 3.0 and it exists as $Hg(OH)_2$ at pH > 5.0. Whereas Hg(II), $HgOH^+$ and $Hg(OH)_2$ exist in the pH range of 3–5 [34]. The low Hg(II) adsorption capacity of MDN observed (Fig. 3) at pH < 3 can be attributed to the competition of H^+ against Hg(II) for the same active sites of the adsorbent. The increase in Hg(II) uptake in the pH range 3–6 can be attributed to the increase in the concentration of $Hg(OH)_2$ in the solution. The Hg(II) adsorption data in the pH range 6–9 (adsorption maxima) indicates $Hg(OH)_2$ is the principal Hg(II) adsorbate. A small reduction in the adsorption capacity observed at pH 10 can be attributed to the increased concentration of OH^- in solution and the competition between $Hg(OH)_2$ and OH^- for the same active site of the adsorbent [14]. These observations are consistent with that of Kim, et al. [35] for Hg(II) removal from aqueous solution using different oxide adsorbents. The XPS and XRD data revealed the presence of HgO on MDN after Hg(II) adsorption. A similar finding has been reported by Collins et al. [36] for the removal of Hg(II) from aqueous solutions using goethite.

The reduced adsorption capacity of Hg(II) from industrial effluent by MDN can be attributed to the interference of co-existing ions like Na^+, Ca^{2+}, Mg^{2+}, Cl^-, etc. In the presence of Cl^-, $HgCl_2$, HgOHCl and $Hg(OH)_2$ are the main solution species of Hg(II). The little or no affinity of Hg(II)–Cl species to the oxide surface may be one other reason for the reduced adsorption capacity as suggested by Yin et al. [37]. The ions induced agglomeration of nanomanganese oxide and thereby increased particle size could also reduce the active adsorption sites.

4. Conclusions

The present study shows that nanostructured MnO_2 prepared through the reduction of potassium permanganate by ethyl alcohol is a very effective adsorbent for Hg(II) removal from aqueous medium and chlor-alkali industrial effluent. Adsorption was found to dependent on Hg(II) concentration, temperature and pH of the system, and the optimum pH was found to be in the range of 6–9. The removal of Hg(II) followed pseudo-second-order kinetics and the equilibrium data followed Langmuir isotherm equation. The experimental evidence suggests that electrostatic force plays dominant role in the adsorption process. The process is endothermic, spontaneous and Hg(II) uptake decreases with increase in ionic strength. The difficulty in handling MDN can be overcome by supporting it on a suitable substrate like Al_2O_3, and such material can act as an effective material for Hg(II) uptake from aqueous solutions and chlor-alkali industrial effluents. The spent adsorbent can be effectively regenerated and reused by acid treatment.

Supplementary data

TEM image of MDN after Hg(II) adsorption, SEM images of MDN before and after Hg(II) adsorption, SEM images of Al_2O_3 and MDN@Al_2O_3, X-ray elemental maps and EDAX spectrum of MDN@Al_2O_3, XRD pattern of MDN before and after Hg(II) adsorption, effect of initial Hg(II) concentration on distribution coefficient, effect of contact time on Hg(II) adsorption, pseudo-first-order reaction kinetic plots for the adsorption of Hg(II) on MDN, isotherm model fits for the adsorption of Hg(II) by MDN at 293 and 313K, R_L values for the adsorption of Hg(II) by MDN, thermodynamic plot for the adsorption of Hg(II) by MDN, D–R isotherm plot, effect of Al_2O_3 dose on the removal of Hg(II) from Hg(II) spiked distilled water and simulated industrial effluent.

Acknowledgement

We thank Department of Science and Technology, Government of India for constantly supporting our research program on nanomaterials.

Appendix A. Supplementary data

Supplementary data associated with this article can be found, in the online version, at doi:10.1016/j.cej.2010.03.031.

References

[1] D. Gibicar, M. Horvat, M. Logar, V. Fajon, I. Falnoga, R. Ferrara, E. Lanzillotta, C. Ceccarini, B. Mazzolai, B. Denby, J. Pacyna, Human exposure to mercury in the vicinity of chlor-alkali plant, Environ. Res. 109 (2009) 355–367.

[2] D. Karunasagar, M.V.B. Krishna, Y. Anjaneyulu, J. Arunachalam, Studies of mercury pollution in a lake due to a thermometer factory situated in a tourist resort: Kodaikkanal, India, Environ. Pollut. 143 (2006) 153–158.

[3] F. Zahir, S.J. Rizwi, S.K. Haq, R.H. Khan, Low dose mercury toxicity and human health, Environ. Toxicol. Pharmacol. 20 (2005) 351–360.

[4] R.C. Srivastava, Guidance and Awareness Raising Materials under New UNEP Mercury Programs (Indian Scenario), Centre for Environmental Pollution Monitoring and Mitigation, India, 2004.

[5] A. Oehmen, R. Viegas, S. Velizarov, M.A.M. Reis, J.G. Crespo, Removal of heavy metals from drinking water supplies through the ion exchange membrane bioreactor, Desalination 199 (2006) 405–407.

[6] K.P. Lisha, T. Anshup, Pradeep, Towards a practical solution for removing inorganic mercury from drinking water using gold nanoparticles, Gold Bull. 42 (2009) 58–66.

[7] T. Budinova, N. Petrov, J. Parra, V. Baloutzov, Use of an activated carbon from antibiotic waste for the removal of Hg(II) from aqueous solution, J. Environ. Manage. 88 (2008) 165–172.

[8] S. Babel, T.A. Kurniawan, Low-cost adsorbents for heavy metals uptake from contaminated water: a review, J. Hazard. Mater. B97 (2003) 219–243.

[9] S.M. Maliyekkal, L. Philip, T. Pradeep, As(III) removal from drinking water using manganese oxide-coated-alumina: performance evaluation and mechanistic details of surface binding, Chem. Eng. J. 153 (2009) 101–107.

[10] S.G. Wang, W.X. Gong, X.W. Liu, Y.W. Yao, B.Y. Gao, Q.Y. Yue, Removal of lead(II) from aqueous solution by adsorption onto manganese oxide-coated carbon nanotubes, Sep. Purif. Technol. 58 (2007) 17–23.

[11] A. Agrawal, K.K. Sahu, Kinetic and isotherm studies of cadmium adsorption on manganese nodule residue, J. Hazard. Mater. B137 (2006) 915–924.

[12] W. Zou, R. Han, Z. Chen, Z. Jinghua, J. Shi, Kinetic study of adsorption of Cu(II) and Pb(II) from aqueous solutions using manganese oxide coated zeolite in batch mode, Colloids Surf. A 279 (2006) 238–246.

[13] T. Boonfueng, L. Axe, Y. Xu, T.A. Tyson, Nickel and lead sequestration in manganese oxide-coated montmorillonite, J. Colloid Interface Sci. 303 (2006) 87–98.

[14] P. Thanabalasingam, W.F. Pickering, Sorption of mercury(II) by manganese(IV) oxide, Environ. Pollut. B 10 (1985) 115–128.

[15] S.M. Hasany, M.H. Chaudhary, Investigation of adsorption behaviour of mercury in microamounts on manganese dioxide from aqueous solutions, J. Radioanal. Nucl. Chem. 100 (1986) 307–315.

[16] S.P. Mishra, S.S. Dubey, D. Tiwari, Inorganic particulates in removal of heavy metal toxic ions IX. Rapid and efficient removal of Hg(II) by hydrous manganese and tin oxides, J. Colloid Interface Sci. 279 (2004) 61–67.

[17] T. Pradeep, Anshup, Noble metal nanoparticles for water purification: A critical review, Thin Solid Films 517 (2009) 6441–6478.

[18] V. Subramanian, H. Zhu, B. Wei, Alcohol-assisted room temperature synthesis of different nanostructured manganese oxides and their pseudocapacitance properties in neutral electrolyte, Chem. Phys. Lett. 453 (2008) 242–249.

[19] H. Chen, J. He, Facile synthesis of monodisperse manganese oxide nanostructures and their application in water treatment, J. Phys. Chem. C 112 (2008) 17540–17545.

[20] National Environment Protection Council (NEPC), Guideline on laboratory analysis of potentially contaminated soils, Schedule B (3) (1999). http://www.ephc.gov.au/pdf/cs/cs 03 lab analysis.pdf.

[21] H. Chen, J. He, C. Zhang, H. He, Self-assembly of novel mesoporous manganese oxide nanostructures and their application in oxidative decomposition of formaldehyde, J. Phys. Chem. C 111 (2007) 18033–18038.

[22] J.F. Moulder, W.F. Stickle, Handbook of X-ray Photoelectron Spectroscopy, Published by ULVAC-PH1-Inc., 1995.

[23] P. Humbert, An XPS and UPS photoemission study of HgO, Solid State Commun. 60 (1986) 21–24.

[24] Y.S. Ho, D.A.J. Wase, C.F. Forster, Batch nickel removal from aqueous solution by sphagnum moss peat, Water Res. 29 (1995) 1327–1332.

[25] J. Dong, Z. Xu, F. Wang, Engineering and characterization of mesoporous silica-coated magnetic particles for mercury removal from industrial effluents, Appl. Surf. Sci. 254 (2008) 3522–3530.

[26] S. Lagergren, B.K. Svenska, Zur theorie dersogenannten adsorption geloester stoffe, Vetenskapsakad. Handl. 24 (1898) 1–39.

[27] Y.S. Ho, Review of second-order models for adsorption systems, J. Hazard. Mater. B136 (2006) 681–689.

[28] J. Febrianto, A.N. Kosasih, J. Sunarso, Y.H. Ju, N. Indraswati, S. Ismadji, Equilibrium and kinetic studies in adsorption of heavy metals using biosorbent: a summary of recent studies, J. Hazard. Mater. 162 (2009) 616–645.

[29] Y. Zhao, Y. Chen, M. Li, S. Zhou, A. Xue, W. Xing, Adsorption of Hg^{2+} from aqueous solution onto polyacrylamide/attapulgite, J. Hazard. Mater. 171 (2009) 640–646.

[30] Y.C. Sharma, Thermodynamics of removal of cadmium by adsorption on an indigenous clay, Chem. Eng. J. 145 (2008) 64–68.

[31] A. Sari, M. Tuzen, Biosorption of cadmium(II) from aqueous solution by red algae (*Ceramium virgatum*): equilibrium, kinetic and thermodynamic studies, J. Hazard. Mater. 157 (2008) 448–454.

[32] A. Sari, M. Tuzen, Removal of mercury(II) from aqueous solution using moss (*Drepanocladus revolvens*) biomass: equilibrium, thermodynamic and kinetic studies, J Hazard. Mater. 171 (2009) 500–507.

[33] D.M. Manohar, K.A. Krishnan, T.S. Anirudhan, Removal of mercury(II) from aqueous solutions and chlor-alkali industry wastewater using 2-mercaptobenzimidazole-clay, Water Res. 36 (2002) 1609–1619.

[34] D. Sarkar, M.E. Essington, K.C. Misra, Adsorption of mercury(II) by variable charge surfaces of quartz and gibbsite, Soil Sci. Soc. Am. J. 63 (1999) 1626–1636.

[35] C.S. Kim, J.J. Rytuba, G.E. Brown, EXAFS study of mercury(II) sorption to Fe- and Al-(hydr)oxides I. Effects of pH, J. Colloid Interface Sci. 271 (2004) 1–15.

[36] C.R. Collins, D.M. Sherman, K.V. Ragnarsdottir, Surface complexation of Hg^{2+} on goethite: mechanism from EXAFS spectroscopy and density functional calculations, J. Colloid Interface Sci. 219 (1999) 345–350.

[37] Y. Yin, H.E. Allen, Y. Li, C.P. Huang, P.F. Sanders, Adsorption of mercury by soil: effects of pH, chloride, organic matter, J. Environ. Qual. 25 (1996) 837–844.